The conserved transcriptional regulator CdnL is required for metabolic homeostasis and morphogenesis in *Caulobacter*

Selamawit Abi Woldemeskel[1], Laura Alvarez[2], Allison K. Daitch[1], Rilee Zeinert[3], Anant Bhargava[1], Diego Gonzalez[4], Justine Collier[4], Peter Chien[3], Felipe Cava[2], Erin D. Goley[1]

1: Department of Biological Chemistry, Johns Hopkins University School of Medicine, Baltimore, MD, USA
2: Department of Molecular Biology, Umeå University, Umeå, Sweden
3: Department of Biochemistry and Molecular Biology, University of Massachusetts-Amherst, MA, USA
4: Department of Fundamental Microbiology, Faculty of Biology and Medicine, University of Lausanne, Switzerland

Abstract

Bacterial growth and division require regulated synthesis of the macromolecules used to expand and replicate components of the cell. Transcription of housekeeping genes required for metabolic homeostasis and cell proliferation is guided by the sigma factor σ^{70}. The conserved CarD-like transcriptional regulator, CdnL, associates with promoter regions where σ^{70} localizes and stabilizes the open promoter complex. However, the contributions of CdnL to metabolic homeostasis and bacterial physiology are not well understood. Here, we show that *Caulobacter crescentus* cells lacking CdnL have severe morphological and growth defects. Specifically, Δ*cdnL* cells grow slowly in both rich and defined media, and are wider, more curved, and have shorter stalks than WT cells. Δ*cdnL* cells also have aberrant localization of MreB and CtpS, cytoskeletal proteins required for maintaining proper cell width and curvature and whose function is dependent on metabolites ATP and CTP respectively. These defects arise from transcriptional downregulation of most major classes of biosynthetic genes, leading to significant decreases in the levels of critical metabolites, including pyruvate, α-ketoglutarate, ATP, NAD^+, UDP-N-acetyl-glucosamine, lipid II, and purine and pyrimidine precursors. Notably, we find that Δ*cdnL* cells are glutamate auxotrophs, and Δ*cdnL* is synthetic lethal with other genetic perturbations that limit glutamate synthesis and lipid II production. Our findings implicate CdnL as a global regulator of genes required for metabolic homeostasis that impacts morphogenesis through availability of lipid II and through metabolite-mediated changes in localization of cytoskeletal regulators of cell shape.

37 **Main**

38 In order to replicate, bacterial cells must synthesize enough macromolecules to double in
39 size using nutrients available in their environment. These macromolecules are used to build
40 structural components of the cell such as the membrane and cell wall, to synthesize the multitude
41 of enzymes required for essential biochemical processes, and to duplicate genetic material.
42 Transcriptional control of housekeeping genes encoding factors that carry out these essential
43 functions contributes to maintaining metabolic homeostasis to support growth and development.
44 Transcription initiation of housekeeping genes is achieved by housekeeping sigma factors that
45 direct the core RNA polymerase (RNAP) to their promoter regions[1], but may be co-regulated by
46 other factors, including the CarD-like transcriptional regulator CdnL. CdnL is broadly conserved
47 in bacteria and is best-characterized in *Myxococcus xanthus* and in *Mycobacteria*[2–6]. It localizes
48 to promoter regions where the housekeeping sigma factor resides, directly binds to the RNAP β
49 subunit, stabilizes the open promoter complex, and is required for transcription from rRNA
50 promoters[2,3,5,7]. *Mycobacterium tuberculosis* CarD (the CdnL homolog) is essential for growth in
51 culture, persistence in mice, and survival during genotoxic stress and starvation[2,4]. CdnL is also
52 essential in *M. xanthus*, where its depletion causes cell filamentation[6]. This last observation
53 implies that CdnL-dependent changes in gene expression are required to support proper
54 morphogenesis, at least in *M. xanthus*.

55 Bacterial morphology is maintained by the peptidoglycan (PG) cell wall, which must be
56 expanded and remodeled in a regulated manner to allow growth and division. It lies just outside
57 the inner membrane and is a continuous, covalently-linked structure made of glycan strands
58 crosslinked together by peptide side chains[8]. In addition to giving the cell its stereotyped shape,
59 the cell wall provides physical integrity and prevents cell lysis due to turgor pressure. Different

60 shape features (e.g. cell length, width, or curvature) are specified by spatially and temporally
61 regulated synthesis and remodeling of the PG that is largely orchestrated by cytoskeletal
62 proteins[8,9]. Though the details of PG synthesis and remodeling and its regulation by cytoskeletal
63 proteins has been the subject of intense study for several decades, how PG metabolism is
64 regulated in coordination with nutrient availability and metabolic status of the cell is
65 incompletely understood.

66 Here, we investigate how CdnL affects metabolism, growth, and morphogenesis in the α-
67 proteobacterium *Caulobacter crescentus* (hereafter *Caulobacter*). *Caulobacter* undergoes
68 stereotyped morphological transitions as it progresses through the cell cycle and during
69 adaptation to a variety of stresses, making it an ideal organism to study bacterial
70 morphogenesis[10]. Although it is known that *Caulobacter* CdnL is not required for viability, the
71 consequences of its loss on *Caulobacter* physiology have not been previously characterized[11].
72 Here, we demonstrate that CdnL regulates transcription of biosynthetic genes required for
73 metabolic homeostasis that, in turn, supports proper growth, PG metabolism, and morphology in
74 *Caulobacter*.
75

76 **Results**

77 Δ*cdnL* cells have growth and morphology defects

78 We became interested in *Caulobacter* CdnL through a screen for spontaneous suppressors of a
79 dominant lethal mutant of the cell division protein FtsZ (called FtsZΔCTL) that causes lethal
80 defects in PG metabolism[12]. Specifically, one of the FtsZΔCTL suppressors we identified carried
81 a point mutation in *cdnL* (*CCNA_00690*) encoding an I42N missense mutation that disrupted
82 CdnL protein stability (Supplementary figure 1a). To examine the role of *cdnL* in *Caulobacter*
83 growth and morphogenesis, we deleted it in a clean genetic background and compared growth
84 and morphology to wild type (WT) cells. We found that Δ*cdnL* cells grew more slowly than WT
85 (Figure 1a) and had pleiotropic morphological defects in complex PYE medium (Figure 1b, c).
86 Quantitative analysis of shape differences between WT and Δ*cdnL* cells grown in PYE using
87 CellTool[13] revealed significant differences in two shape modes which approximately correspond
88 to cell curvature (shape mode 2) and cell width (shape mode 3) (Figure 1c). Specifically, we
89 observed that in PYE, Δ*cdnL* cells were wider and more curved than WT cells (Figure 1b, c, d).
90 In these shape modes, Δ*cdnL* cells were also more variable in their range of values than WT,
91 indicating less precise maintenance of shape in the mutant (Figure 1c). Additionally, we
92 observed phase-light "ghost" cells in Δ*cdnL* samples indicative of cell lysis and suggesting a lack
93 of integrity in the cell envelope (Figure 1b, arrows).

94 To further characterize the Δ*cdnL* growth and morphology phenotypes, we grew WT and
95 Δ*cdnL* cells in the defined media M2G or HIGG. Surprisingly, we found that M2G was unable to
96 support growth of cells lacking CdnL, but that Δ*cdnL* cells grew in HIGG, albeit more slowly
97 than WT (Figure 1a). A comparison of the components of M2G and HIGG media suggested that
98 the missing nutrient in M2G that is required for growth of Δ*cdnL* cells might be glutamate.

99 Consistent with this, addition of sodium glutamate to M2G (called M2GG with sodium
100 glutamate added) supported growth of Δ*cdnL* cells to a similar rate as in HIGG. These data
101 indicate that Δ*cdnL* cells are unable to synthesize sufficient glutamate to support growth and are
102 now glutamate auxotrophs (Figure 1a). No other amino acids are included in either M2G or
103 HIGG, suggesting a specific requirement for exogenous glutamate.
104 Similar to our observations with PYE, we found that Δ*cdnL* cells grow more slowly than
105 WT in M2GG or HIGG and also had aberrant shape (Figure 1a, b). Δ*cdnL* cells were again
106 hypercurved and wider than WT cells, but unlike in PYE, Δ*cdnL* cells were also consistently
107 shorter than WT in each defined medium (Figure 1b, c, d). The polar stalk is a prominent
108 morphological feature of *Caulobacter* cells and, like other features of cell shape, stalk biogenesis
109 and elongation requires PG synthesis[14]. Since we observed stereotyped shape changes in cells
110 lacking CdnL, we also compared stalk morphogenesis between WT and Δ*cdnL* cells. We found
111 that in phosphate replete HIGG media (containing 200 μM PO_4^-) Δ*cdnL* cells had short stalks
112 compared to WT cells (Figure 1e, f), suggesting that CdnL impacts all aspects of morphogenesis
113 in *Caulobacter*. Stalks elongate in response to phosphate starvation in *Caulobacter* through a
114 pathway that is distinct from developmentally regulated stalk morphogenesis. Interestingly,
115 Δ*cdnL* cells significantly elongated their stalks during phosphate starvation (Figure 1 e, f)
116 suggesting that Δ*cdnL* cells can still alter their morphology in response to phosphate starvation.
117
118 <u>MreB is hyperfocused at midcell in Δ*cdnL* cells</u>
119 In bacteria, cytoskeletal proteins spatially regulate cell wall synthesis required for shape
120 determination and maintenance[10]. To investigate if the shape defects that we observe in Δ*cdnL*
121 arise due to changes in levels of cytoskeletal proteins, we probed for changes in levels of MreB,

122 FtsZ, crescentin, and CTP synthase and found no differences in protein or transcript levels
123 between Δ*cdnL* and WT cells (Supplementary table 1 and data not shown).
124 Since Δ*cdnL* cells had significant differences in width and curvature, we focused on the
125 cytoskeletal proteins that determine these shape features. In bacteria, the actin homolog and
126 ATPase MreB is required for rod shape, width maintenance, and cell body elongation[15,16].
127 Additionally, MreB influences curvature of *Caulobacter* cells through its effects on the
128 intermediate filament-like protein, crescentin[17]. To determine if the localization of MreB is
129 altered in Δ*cdnL*, we expressed *venus-mreB* from the *xylX* promoter and visualized MreB
130 localization in WT or Δ*cdnL* cells grown in PYE, M2G, and HIGG media (Figure 2 a,b,c). In
131 WT cells grown in PYE, MreB has a patchy localization along the length of the cell in newborn
132 swarmer (G1) cells, shifts to midcell in stalked (S) and early predivisional cells, and assumes a
133 patchy localization in late predivisional cells[15]. Interestingly, we found that the localization of
134 MreB at midcell is more tightly focused in Δ*cdnL* cells compared to WT in all three media tested
135 (Figure 2a,b,c). Moreover, we found that most WT cells localize MreB along the length of the
136 cell when grown in HIGG media (Figure 2c). However, the localization of MreB in HIGG shifts
137 to mostly at midcell when *cdnL* is deleted. To better visualize the localization of MreB across
138 populations and throughout the cell cycle, we created demographs. In cells that have MreB
139 localized at midcell, we found that the localization of MreB is more tightly focused with minimal
140 signal outside of the midcell region (Figure 2d,e,f). To quantitatively compare the differences in
141 MreB localization between WT and Δ*cdnL*, we fit the MreB signal at midcell to an eight term
142 Fourier series model and calculated the full width at half max (FWHM). We found that the
143 FWHM at midcell is smaller in Δ*cdnL* cells compared to WT, consistent with what we inferred
144 from the images and demographs (Figure 2g,h,i).

145 To further characterize the link between MreB localization and loss of *cdnL,* we deleted
146 *cdnL* in backgrounds that have mutations near the ATP binding pocket of MreB. These
147 mutations cause MreB to localize at the poles, along the length of the cell, or at midcell
148 throughout the cell cycle[17]. These aberrant localizations of MreB cause changes in cell shape but
149 do not affect growth rate (Supplementary figure 2a,b,c). Deletion of *cdnL* in each of these
150 backgrounds caused severe morphological and growth defects (Supplementary figure 2a,b). The
151 severity of growth and shape defects was worse in mutant backgrounds that do not localize MreB
152 to midcell (Supplementary figure 2). Interestingly, we found that MreB V324A, which has a
153 patchy localization in a WT background, becomes enriched at midcell when *cdnL* is deleted and
154 grows similarly to mutants that localize MreB to midcell (Supplementary figure 2b,c,d,e). These
155 data suggest that localization of MreB at midcell is important for fitness in Δ*cdnL* cells. Since
156 MreB is essential for specification and maintenance of width and curvature, the mislocalization
157 of MreB may contribute to the width and curvature defects that we observe in Δ*cdnL.*
158
159 <u>Hypercurvature of Δ*cdnL* cells is dependent on crescentin and may involve CTP synthase</u>
160 In *Caulobacter*, crescentin drives the patterning of PG synthesis required for cell curvature[9,18].
161 To determine if hypercurvature of Δ*cdnL* cells is dependent on crescentin, we deleted *cdnL* in a
162 Δ*creS* background. We observed that Δ*cdnL*Δ*creS* cells are straight, indicating that
163 hypercurvature is dependent on crescentin (Figure 3a,b). In addition to crescentin, curvature is
164 influenced by the metabolic enzyme CTP synthase (CtpS), which forms filaments near crescentin
165 when CTP is abundant and negatively regulates curvature in a crescentin-dependent manner[19,20].
166 Since we observed that Δ*cdnL* cells are hypercurved, we hypothesized that the hypercurvature of
167 Δ*cdnL* may arise due to fewer CtpS filaments. Thus, we expressed *mcherry-ctpS* from the

168 xylose-inducible promoter in WT or Δ*cdnL* cells and visualized localization of CtpS filaments
169 and found that Δ*cdnL* cells form fainter CtpS filaments compared to WT (Supplementary figure
170 3). Additionally, demograph analysis of mCherry-CtpS localization indicated that mCherry-CtpS
171 forms less robust filaments and has more dispersed signal in Δ*cdnL* cells grown in PYE or
172 M2GG compared to WT (Figure 3c, Supplementary figure 3). Thus, our data suggest that
173 formation of fewer CtpS filaments in Δ*cdnL* cells may lead to the hypercurvature phenotype that
174 we observe.
175
176 Genes involved in biosynthetic processes are downregulated in Δ*cdnL*
177 Having established that the transcriptional regulator CdnL plays a role in growth and
178 morphogenesis and influences the localization of morphogenetic proteins, we next sought to
179 understand how it exerts these effects. To identify genes that are misregulated in Δ*cdnL* that may
180 be responsible for the growth and morphology defects that we observe, we extracted mRNA from
181 WT and Δ*cdnL* cells and performed RNA-Seq. The results from this analysis showed that
182 approximately 30% of the transcriptome is misregulated in cells lacking CdnL (Supplementary
183 table 1). A closer look at genes that are downregulated in the Δ*cdnL* clone that we used for RNA-
184 seq analysis suggested that a 50 kbp region comprising 51 genes between CCNA_02773 and
185 CCNA_02826 was highly downregulated in Δ*cdnL*. This region is flanked by identical sequences
186 that encode transposases CCNA_02772 and CCNA_02828, suggesting that this region may be
187 deleted in the Δ*cdnL* clone (EG1415) used in our RNA-seq analysis. Indeed, deletion of this region
188 was confirmed by PCR. However, we found no differences in growth or morphology between the
189 Δ*cdnL* clone with the 50 kbp deletion (EG1415, Δ50kbp) and Δ*cdnL* clones containing this region
190 (e.g. EG1447), indicating that this region does not contribute significantly to the growth and shape

191 defects that we observe (Supplementary figure 1b, c). Previously, this region of the chromosome
192 was shown to be readily lost in a background lacking the methyltransferase *ccrM*[21]. Similar to our
193 observations with Δ*cdnL*, loss of this region in Δ*ccrM* did not yield any specific growth
194 advantages. To ensure that loss of this region did not impact our analysis of the transcriptional
195 consequences specific to deleting *cdnL*, we analyzed the transcriptome of an independent Δ*cdnL*
196 clone that has the 50 kbp region intact (JC784) by microarray analysis (Supplementary table 1).
197 We found significant overlap between our RNA-Seq dataset using EG1415 and microarray dataset
198 using JC784 (Supplementary figure 1d, e, f, g). We generally used the intersection of our two
199 datasets (RNA-Seq of EG1415 and microarray of JC784) as a conservative and rigorous
200 representation of the consequences of deleting *cdnL* on the *Caulobacter* transcriptome.
201 To obtain an overview of how loss of CdnL affects the transcriptome we used DAVID[22]
202 functional annotation analysis to functionally categorize genes that had at least a two-fold change
203 in transcript abundance in Δ*cdnL* in both the RNA-Seq and microarray datasets (Supplementary
204 table 2). Of the genes that are downregulated in Δ*cdnL*, we found an overrepresentation of genes
205 involved in biosynthetic and bioenergetic pathways including amino acid, nucleotide, fatty acid,
206 lipid, cell wall, cell membrane, and central carbon metabolism. Genes that are over 2-fold
207 upregulated in Δ*cdnL* clustered into categories involved in transcription, transport, and motility.
208
209 <u>Δ*cdnL* cells have reduced levels of central carbon and TCA metabolites required for synthesizing</u>
210 <u>macromolecules critical for growth</u>
211 Since our transcriptome analysis revealed downregulation of pathways involved in
212 macromolecular biosynthesis, we hypothesized that Δ*cdnL* cells may have limited amounts of
213 substrates available for proliferative processes. To identify how the metabolome changes when

214 *cdnL* is deleted, we extracted metabolites from WT and Δ*cdnL* cells grown in PYE, M2GG,
215 M2G (grown in M2GG, washed and grown in M2G for 12 hours) or HIGG media or CdnL-
216 depleted cells grown in PYE and performed LC/MS analysis of polar metabolites. Consistent
217 with what we inferred from our transcriptomic data, we found glycolytic and tricarboxylic acid
218 (TCA) intermediates, amino acids, nucleotides, and their derivatives to be significantly altered,
219 suggesting that central carbon metabolism and carbohydrate utilization is reduced in cells lacking
220 CdnL (Figure 4, Supplementary table 3 & Supplementary figure 4). Specifically, we found
221 biosynthetic precursors and cofactors such as pyruvate, NAD^+, ATP, and UDP-N-acetyl
222 glucosamine are significantly reduced in Δ*cdnL* cells while D-xylose, uric acid, the TCA
223 intermediates fumarate and malate, the pyrimidine and amino acid precursor dihydroorotate, the
224 leucine synthesis intermediate 2-isopropylmalic acid, and the storage molecule 3-hydroxybutyric
225 acid are significantly higher in Δ*cdnL* across all conditions compared to WT (Figure 4,
226 Supplementary table 3 & Supplementary figure 4). The presence of higher uric acid across all
227 media suggests that Δ*cdnL* cells are preferentially catabolizing amino acids rather than
228 carbohydrates as a carbon source.

229 Since we performed our transcriptomics analysis in PYE, we compared our RNA-Seq
230 data to our PYE metabolome dataset. In *Caulobacter*, glucose is metabolized to yield substrates
231 that feed into the TCA cycle via the Entner-Doudoroff pathway[23,24]. Since intermediates in and
232 products of this glycolytic pathway are reduced in Δ*cdnL*, we looked at our transcriptomic data
233 to see if the levels of transcripts encoding any of the enzymes in this pathway are changed. We
234 found that *CCNA_01562* and *CCNA_01560* are significantly downregulated suggesting that
235 disruption in flux through the Entner-Doudoroff pathway may, indeed, lead to low levels of
236 pyruvate and phosphoenolpyruvate (PEP) (Figure 4b, Supplementary table 1). WT *Caulobacter*

237 can synthesize all amino acids *de novo* using TCA cycle intermediates[23]. During growth in media
238 without amino acids, *Caulobacter* cells can convert PEP to oxaloacetate to replenish TCA
239 intermediates[23]. We found that *CCNA_01560*, which converts PEP to oxaloacetate, is also highly
240 downregulated in Δ*cdnL*. Thus, our observations of low α-ketoglutarate levels and glutamate
241 auxotrophy may arise due to reduced flux of pyruvate and PEP into the TCA cycle (Figure 4).
242 Interestingly, D-xylose levels were elevated in Δ*cdnL* cells in all media tested, although xylose
243 was not provided exogenously. Conversely, genes required to metabolize xylose are
244 downregulated in Δ*cdnL*. Previously, xylose accumulation without an ability to metabolize
245 xylose has been shown to upregulate isocitrate lyase (*CCNA_01841*) and initiate the glyoxylate
246 bypass which promotes conversion of isocitrate to succinate, bypassing key TCA cycle
247 intermediates such as α-ketoglutarate.[23,25] Additionally, upregulation of malate synthase
248 (*CCNA_01843*) combines glyoxylate produced by isocitrate lyase to acetyl-coenzyme A to
249 produce malate, allowing a modified TCA cycle to continue.[23] Consistently, we find that
250 *CCNA_01841* and *CCNA_01843* are over four-fold and two-fold upregulated in Δ*cdnL*,
251 respectively (Supplementary table 1), suggesting low levels of α-ketoglutarate may arise due to
252 activation of the glyoxyate bypass in addition to low levels of pyruvate and PEP. Since α-
253 ketoglutarate is used to synthesize glutamate (Figure 4b), the glutamate auxotrophy of Δ*cdnL*
254 cells may arise due to low amounts α-ketoglutarate produced by the TCA cycle. Additionally,
255 we found that *gdhA* and *gltB*, genes essential for glutamate biosynthesis from α-ketoglutarate or
256 glutamine, are over 4-fold downregulated in our transcriptomic analysis (Figure 5a,
257 Supplementary table 1). Collectively, our data indicate that changes in the transcriptome that
258 arise when *cdnL* is deleted have detrimental consequences on metabolic pathways disrupting

259 levels of key metabolites required for energy production and amino acid and nucleotide
260 biosynthesis.
261
262 Δ*cdnL* cells have low levels of the cell wall precursor and changes in cell wall crosslinking
263 Our metabolomics analysis showed that UDP-N-acetylglucosamine and PEP, substrates required
264 for synthesis of the PG precursor lipid II, are significantly lower in Δ*cdnL* compared to WT
265 (Figure 4). Additionally, our transcriptomic analysis indicated that genes required for lipid II
266 biosynthesis are highly downregulated (Figure 5a) leading us to postulate that PG material
267 maybe limiting in Δ*cdnL* cells. Since PG synthesis is required for both cell shape maintenance
268 and cell envelope integrity, changes in abundance of lipid II might underlie the shape and cell
269 lysis phenotypes observed for Δ*cdnL* cells. We directly compared lipid II levels in WT and
270 Δ*cdnL* cells and found that Δ*cdnL* cells have a striking 45% reduction in lipid II levels as
271 compared to WT (Figure 5b).
272 To assess if CdnL-mediated changes in transcription result in alterations to PG metabolic
273 activities in addition to lipid II synthesis, we performed muropeptide analysis on PG isolated
274 from WT and Δ*cdnL* cells to identify changes in PG chemistry. Consistent with low levels of
275 lipid II, Δ*cdnL* cells have 23% less PG polymer than WT (Figure 5c). Although overall PG
276 crosslinking is unaffected, Δ*cdnL* cells had significantly more dimers and fewer trimers (higher
277 order crosslinks) than WT (Figure 5d, Supplementary Figure 5). The mutant also shows an
278 increased chain length, as the relative amount of anhydro muropeptides (glycan chain termini)
279 were significantly reduced in Δ*cdnL* cells (Figure 5d, Supplementary Figure 5). Moreover,
280 Δ*cdnL* cells had more pentapeptides and glycine-containing muropeptides compared to WT
281 (Figure 5d, Supplementary Figure 5). Thus, the shape and envelope integrity defects observed in

282 Δ*cdnL* cells may arise, at least in part, from a combination of low levels of lipid II and significant
283 changes in the chemical structure of the cell wall.
284
285 Pathways impacting PG metabolism become essential in Δ*cdnL*
286 To gain insight into which transcriptional and metabolic changes in Δ*cdnL* may be most relevant
287 to fitness, we performed comparative transposon sequencing (Tn-Seq) on WT and Δ*cdnL* strains.
288 Consistent with morphological defects and low amounts of lipid II observed for Δ*cdnL* cells, we
289 found several normally non-essential genes involved in pathways that interact with PG synthesis
290 could not be disrupted in the Δ*cdnL* background (Figure 6a, Supplementary table 4).
291 Specifically, we identified genes involved in glutamate metabolism, PG metabolism, PG
292 recycling, and capsule synthesis in which we recovered far fewer transposon insertions in the
293 Δ*cdnL* background than in WT (Figure 6a,b, Supplementary table 4). Of the genes involved in
294 glutamate metabolism, GdhZ and MurI become essential in Δ*cdnL*. Each of these proteins link
295 glutamate metabolism to morphogenesis: MurI by making D-Glu for lipid II synthesis and GdhZ
296 via its effects on the morphogenetic protein FtsZ[26,27].
297 Our Tn-Seq analysis also indicated that *ampG (CCNA_00136)* and *ampD*
298 (*CCNA_02650*), genes required for PG recycling, become essential in Δ*cdnL* (Figure 6b,
299 Supplementary table 4). AmpG is a permease that allows transport of cell wall material from the
300 periplasm to the cytoplasm and AmpD degrades transported cell wall material to provide
301 building blocks for lipid II synthesis[28]. We attempted to delete *cdnL* in a Δ*ampG* background, but
302 were unable to obtain clones with deletions in both *ampG* and *cdnL*, supporting the genetic
303 interaction suggested from the Tn-Seq. Since lipid II levels are low in Δ*cdnL*, the cell apparently
304 relies on pathways that allow for recycling of the existing cell wall material for survival.

305 In addition to PG metabolic genes, we found putative synthetic lethal interactions
306 between capsule (exopolysaccharide) biosynthetic genes and *cdnL* (Figure 6a,b, Supplementary
307 table 4). During capsule synthesis, saccharide precursors are synthesized on the lipid anchor
308 undecaprenyl phosphate (Und-P) in the cytoplasm, flipped to the periplasmic space, and
309 assembled into a polysaccharide that is exported to the outer surface of the cell[29]. Thus, PG
310 synthesis and capsule synthesis each use Und-P as a lipid carrier for synthesis and export into the
311 periplasmic space. Previous work in *Escherichia coli* and *Bacillus subtilis* has shown that
312 disruption of pathways that use Und-P can lead to Und-P sequestration and cause severe growth
313 and morphological defects by inhibiting lipid II synthesis[30–32]. Similarly, we propose that
314 disrupting the capsule biosynthesis pathway in *Caulobacter* may sequester Und-P in dead-end
315 intermediates, limiting lipid II synthesis. We attempted to delete each of the capsule genes
316 predicted by Tn-Seq to genetically interact with *cdnL* in Δ*cdnL* cells. We were unsuccessful with
317 the exception of *CCNA_00164*, which encodes a putative O-antigen polymerase ligase and which
318 had the weakest predicted genetic interaction with *cdnL* of the capsule genes (Figure 6a, b and
319 Supplementary table 4). Nevertheless, deletion of both *cdnL* and *CCNA_00164* resulted in cells
320 with morphological defects that are more severe than Δ*cdnL* alone (Figure 6d). Moreover, these
321 double mutant cells grew more slowly than Δ*cdnL* (Figure 6c). Deletion of *CCNA_00164* by
322 itself had no obvious effect on growth or morphology. Our data support the model that mutations
323 in the capsule biosynthesis pathway sequester Und-P and limit its availability for lipid II
324 synthesis, exacerbating the existing lipid II deficiency of Δ*cdnL* cells to a lethal level.
325 Collectively, our transcriptomic data, biochemical analyses, and genetic interaction results
326 indicate that CdnL is required to maintain adequate availability of the PG precursor lipid II to
327 support normal growth and morphology.

328 Discussion

329 In this work, we unveil a new role for the conserved, global transcriptional regulator
330 CdnL in mediating transcription of biosynthetic genes required for metabolic homeostasis in
331 *Caulobacter*. We show that in Δ*cdnL* cells, transcription of many classes of biosynthetic genes is
332 downregulated, with physiologically critical defects in glutamate and lipid II metabolism, in
333 particular. These changes in metabolic pools affect growth and morphology directly by limiting
334 macromolecules required for cell growth and envelope expansion, and indirectly by influencing
335 morphogenetic proteins. Downregulation of genes involved in biosynthetic and bioenergetics
336 pathways in Δ*cdnL* cells, an altered metabolic landscape in Δ*cdnL*, and the reliance of Δ*cdnL*
337 cells on exogenous glutamate, which is a central node in multiple biosynthetic pathways,
338 establish CdnL as a global regulator of genes required for central metabolism and
339 macromolecular synthesis[33,34].

340 Previously, CdnL has been shown to directly bind to RNAP and stabilize the open
341 promoter complex required for transcription of rRNA promoters in *Mycobacteria* and *M.*
342 *xanthus*[3,5]. Similarly, *Caulobacter* CdnL has been shown to bind RNAP and regulate
343 transcription from an rRNA promoter[11]. Here, we demonstrate that loss of CdnL has global
344 effects on various aspects of bacterial metabolism. Interestingly, however, transcriptomic
345 changes that occur during loss of CdnL in *Caulobacter* are, in many aspects, the opposite of what
346 is observed in *Mycobacterium smegmatis*. CarD depletion in *M. smegmatis* leads to upregulation
347 of genes encoding the translation machinery and enzymes in metabolic pathways such as amino
348 acid biosynthesis and to downregulation of genes involved in degradation of amino acids, fatty
349 acid metabolism and membrane proteins[2]. Although loss of CdnL generally has opposite effects
350 on expression of metabolic genes in these two divergent bacteria, CdnL-mediated effects on the

351 transcriptome impact proliferative and metabolic processes and are thereby essential for proper
352 growth in *Caulobacter* and viability in *Mycobacteria*.

353 In *Caulobacter*, loss of CdnL causes aberrant morphogenesis, at least in part, by limiting
354 production of lipid II. The effects of *cdnL* deletion are in some ways reminiscent of loss of the
355 master regulator and RNA chaperone Hfq in *Caulobacter*[35]. Deletion of *hfq* alters the levels of
356 several metabolites, including glutamate and components of the TCA cycle. Importantly, this
357 includes accumulation of α-ketoglutarate which, in turn, causes reduced synthesis of lipid II and
358 pleiotropic cell shape defects[35]. Though both Hfq and CdnL are required to maintain sufficiently
359 high levels of lipid II to support growth and stereotyped cell shape, CdnL has a distinct shape
360 phenotype, likely mediated by additional impacts on MreB and CtpS.

361 In recent years, a growing number of factors have been described that link the metabolic
362 status of the cell to morphology through cytoskeletal proteins [8,34,36]. The best-studied examples
363 of this employ moonlighting functions of metabolic enzymes to couple metabolism to
364 morphology. For example, the glucosyltransferases UgtP and OpgH in *B. subtilis* and *E. coli,*
365 respectively, alter FtsZ dynamics and affect cell size in a UDP-glucose dependent manner[37,38].
366 Similarly, in *Caulobacter* GdhZ and KidO alter FtsZ assembly in a glutamate-dependent manner,
367 coupling metabolism to cell division[26,39]. In the case of CdnL, its impact on the localization of
368 the cytoskeletal proteins MreB and CtpS may be metabolite-mediated rather than protein-
369 mediated. Polymerization of CtpS into filaments that negatively regulate cell curvature is
370 dependent on CTP, which is predicted to be present in low amounts in Δ*cdnL* cells by both our
371 transcriptomic and metabolomic analyses (Fig. 4a and Supplementary table 1). It is unclear how
372 MreB localization is regulated in *Caulobacter*, though it appears to be linked to its ATP-
373 dependent polymerization cycle[17] and may involve cell wall precursors. Thus, we propose that

374 the disruption of metabolic homeostasis that arises from loss of CdnL impacts morphology
375 through metabolite-mediated effects on cytoskeletal proteins in addition to reduced levels of lipid
376 II.

377 Interestingly, depletion of CdnL in *M. xanthus* results in cell filamentation, consistent
378 with a conserved impact on morphogenesis[6]. The effects, if any, of CarD depletion in
379 *Mycobacteria* on cell morphology have not been reported, nor have the effects of CdnL depletion
380 on the *M. xanthus* transcriptome or metabolome. Future work in diverse organisms will reveal if
381 the role of CdnL as a global regulator of both morphogenesis and metabolism is conserved
382 across bacteria.

383 Methods

384 **Bacterial strains, plasmids, growth conditions**

385 *Caulobacter crescentus* NA1000 strains were grown in peptone yeast extract medium (PYE) ,
386 M2G[40], M2GG (M2G with 0.15% sodium glutamate), or Hutner base imidazole-buffered glucose
387 glutamate medium (HIGG)[41]. Xylose was used at 0.3% for induction experiments. EG1415 and
388 JC874 were used for RNA-Seq and microarray experiments, respectively. All other experiments
389 with Δ*cdnL* were performed using EG1447 (clean, in-frame deletion of *cdnL*) or EG1898 (*cdnL*
390 coding sequence replaced with *aacC1,* conferring gentamicin resistance) or derivatives thereof.
391 JC874, EG1447, and EG1898 contain the 50 kb region that is deleted in EG1415. Growth curves
392 were performed at 30 ^{o}C in a Tecan Infinite M200 Pro plate reader, 100 µL culture volume, with
393 each strain monitored in biological triplicate at OD_{600} every 30 min with intermittent shaking.
394 Antibiotics for growing *Caulobacter* and cloning and *E. coli* were used at concentrations in
395 liquid (solid) media as described in Woldemeskel *et al* 2017[42]. *C. crescentus*: kanamycin 5 (25)
396 µg/mL, gentamicin 1 (5) µg/mL. *E. coli:* ampicillin 50 (100) µg/mL, kanamycin 30 (50) µg/mL,
397 gentamicin 15 (20) µg/mL, and spectinomycin 50 (50) µg/mL.

398 **Phase contrast, ensemble fluorescence microscopy and image analysis**

399 Cells in exponential phase of growth were spotted on 1% agarose pads and imaged using a Nikon
400 Eclipse Ti inverted microscope equipped with a Nikon Plan Fluor 100X (NA1.30) oil Ph3
401 objective and Photometrics CoolSNAP HQ^2 cooled CCD camera. Chroma filter cubes ET-EYFP
402 and ET-dsRED were used for Venus and mCherry, respectively. Images were processed using
403 Adobe Photoshop and demographs were made using Oufti[43]. Principal component analysis to
404 identify shape variations were performed using CellTool[13] after phase contrast images were
405 converted to binary masks in ImageJ[44] and edited in Adobe Photoshop to remove overlapping

406 cells. Full-width at half-maximum (FWHM) calculations of midcell MreB signal from Oufti[43]
407 output were performed using a custom MATLAB script which fit the normalized signal output
408 from Oufti[43] into an eighth term Fourier series model. Cells for which the fit had adjusted R
409 square value greater than 0.85 were chosen for FWHM calculation. Cells that have midcell
410 localized MreB were selected for FWHM determination based on cell length bins guided by
411 demographs.

412 **Immunoblotting to assess CdnL levels**

413 His_6-SUMO-CdnL was overproduced in Rosetta (DE3) pLysS *E.coli* cells from pEG1129 by
414 inducing for 3 h at 30 ºC with 0.5 mM IPTG at OD_{600} of 0.5. Cells were harvested by
415 centrifugation, resuspended in lysis buffer (50 mM Tris-HCl, pH 8.0, 300 mM KCl, 20 mM
416 imidazole, and 10% glycerol), lysed with 1 mg/mL lysozyme, sonicated and centrifuged at 4 ºC
417 for 30 min at 15000 x g. Supernatant was loaded onto a HisTrap FF 1 mL column (GE Life
418 Sciences) and eluted with lysis buffer with 300 mM imidazole, cleaved with His_6-Ulp1 (SUMO
419 protease) at 1:500 (protease: fusion) molar ratio overnight while dialyzing into lysis buffer.
420 Sample was reloaded onto HisTrap FF 1mL and flow through collected to separate His_6-SUMO
421 and His_6-Ulp1 from CdnL. CdnL fraction was dialyzed into PBS prior to antibody production.
422 Cells in log phase were isolated and lysed in SDS-PAGE loading buffer by boiling for 5 min.
423 Standard procedures were used for SDS-PAGE and transfer to nitrocellulose membrane. CdnL
424 antisera was generated by immunizing a rabbit with CdnL purified as above (Pocono Rabbit
425 Farm & Laboratory). Specificity was determined using cell lysates with deleted or overexpressed
426 *cdnL*. CdnL antisera was used at 1:5000.

427 **RNA-Seq preparation**

428 Cultures of three independent colonies of WT (EG865) and Δ*cdnL* (EG1415, Δ50kb) cells were
429 grown in PYE and harvested at OD_{600} of 0.45 and total RNA was extracted using PureLink RNA
430 Mini Kit from Thermo Fisher using the protocol provided with the kit. Briefly, cells were
431 harvested, lysed, and homogenized using lysozyme, SDS, provided Lysis buffer, and homogenizer.
432 Nucleic acids were extracted with ethanol and loaded onto the provided spin cartridge. DNA-free
433 total RNA was extracted using the on-column PureLink DNAse Treatment protocol. PureLink
434 DNAse mixture was directly added on to the spin cartridge membrane, incubated for 15 min and
435 washed using provided wash buffers and RNA was eluted with RNAse-free water. Finally, RNA
436 quality was quantified using a bioanalyzer and rRNA was removed using the Ribo-Zero rRNA
437 Removal Kit (Gram-Negative Bacteria). RNA-Seq libraries were prepared using the Illumina
438 TruSeq stranded RNA kit and sequenced on an Illumina HiSeq 2500. Data analysis was performed
439 using the Illumina's CASAVA 1.8.2, Bowtie2 (v 2.2.5), and Bioconductor's DESeq package.
440 rRNA clean up, quality control analysis, library prep, sequencing and analysis was performed by
441 the Johns Hopkins University School of Medicine Next Generation Sequencing Center.

442 **Microarray preparations**

443 Biological triplicates of WT (JC450) and Δ*cdnL* (JC784) cultures grown in PYE were harvested
444 at OD_{660} of 0.3. RNA was extracted with Trizol, purified using Ambion PureLink RNA mini-kit
445 according to manufacturer's protocol. Double stranded cDNA was prepared with Roche Double
446 Stranded cDNA synthesis kit. Microarray analysis was performed on Nimblegen custom chips
447 following the manufacturer's protocol for labeling, hybridization on 4-plex chips, and washing.
448 Scanning was performed with Agilent microarray scanner at 3 μm and normalization was
449 performed with Nimblescan implemented RMA algorithm (3 x 4-plex chips in total, all samples
450 from the same culture conditions). The statistical analysis of significance was performed with R

451 using the Significance of Analysis of Microarrays (SAM) method implemented in the library
452 *siggenes.*[45]

453 **DAVID analysis and functional clustering**

454 Genes with a two-fold change in transcript levels in both RNA-Seq and microarray analysis were
455 functionally categorized using DAVID[22] with a medium classification stringency and default
456 parameters.

457 **Transposon library preparation, sequencing, and analysis**

458 Two Tn-Seq libraries each were generated for WT (EG865) and Δ*cdnL* (EG1447). 1L PYE
459 cultures were harvested at OD_{600} of 0.4-0.6, washed 5 times with 10% glycerol, and
460 electroporated with the Ez-Tn5 <Kan-2> transposome (Epicentre). Cells were recovered for 90
461 minutes at 30 ºC with shaking, and plated on PYE-Kan plates. WT libraries were grown for 5
462 and 6 days and Δ*cdnL* libraries were grown for 6 and 10 days. Colonies were scraped off plates,
463 combined, resuspended to form a homogeneous solution in PYE, and flash frozen in 20%
464 glycerol. Genomic DNA for each library was extracted from an aliquot using the DNeasy Blood
465 and Tissue Kit (Qiagen). Libraries were then prepared for Illumina Next-Generation sequencing
466 through sequential PCR reactions. The first PCR round used arbitrary hexamer primers with a
467 Tn5 specific primer going outward. The second round used indexing primers with unique
468 identifiers to filter artifacts arising from PCR duplicates. Indexed libraries were pooled and
469 sequenced at the University of Massachusetts Amherst Genomics Core Facility on the NextSeq
470 550 (Illumina).

471 Sequencing reads were first demultiplexed by index, each library was concatenated and clipped
472 of the molecular modifier added in the second PCR using Je[46]:

473 java -jar /je_1.2/je_1.2_bundle.jar clip F1=compiled.gz LEN=6

474 Reads were then mapped back to the *Caulobacter crescentus* NA1000 genome (NCBI Reference
475 Sequence: NC_011916.1) using BWA[47] and sorted using Samtools[48]:
476 bwa mem -t2 clipped.gz | samtools sort -@2 - > sorted.bam
477 Duplicates were removed using Je[46] and indexed with Samtools[48] using the following command:
478 java -jar /je_1.2/je_1.2_bundle.jar markdupes I=sorted.bam O=marked.bam M=METRICS.txt
479 MM=0 REMOVE_DUPLICATES=TRUE
480 samtools index marked.bam
481 The 5' insertion site of each transposon were converted into .wig files comprising of counts per
482 position and visualized using Integrative Genomics Viewer (IGV)[49,50]. Specific hits for each
483 library were determined with coverage and insertion frequency using a bedfile containing all
484 open reading frames from NC_011916.1 and the outer 20% of each removed to yield a clean and
485 thorough insertion profile. This was determined using BEDTools[51,52] and the following
486 commands:
487 bedtools genomecov -5 -bg marked.bam > marked.bed
488 bedtools map -a NA1000.txt -b marked.bed -c 4 > output.txt
489 Library comparisons were performed using the edgeR package in the Bioconductor suite using a
490 quasi-likelihood F-test (glmQLFit) to determine the false discovery rate adjusted p-values
491 reported here.
492 **Lipid II extraction and analysis**
493 Precursor extraction was performed as described previously and performed in triplicates[53].
494 Briefly, 500 mL of WT and Δ*cdnL* were grown in PYE to OD_{600} of 0.45. Cells were harvested,
495 resuspended in 5 mL PBS and poured into 50 mL flasks containing 20 mL $CHCl_3$:Methanol
496 (1:2). The mixture was stirred for 1 h at room temperature and centrifuged for 10 min at 4000 x g

497 at 4 ºC. The supernatant was transferred to clean 250 mL flasks containing 12 mL $CHCl_3$ and 9
498 mL PBS, stirred for 1 h at room temperature and centrifuged for 10 min at 4000 x g at 4 ºC. The
499 interface fraction (between the top aqueous and bottom organic layers) was collected and
500 vacuum dried. To remove lipid tail, samples were resuspended in 100 µL DMSO and 800 µL
501 H_2O, 100 µL ammonium acetate 100 mM pH 4.2 were added. This mixture was boiled for 30
502 min, dried in vacuum and resuspended in 300 µL H_2O. Samples were analyzed by UPLC
503 chromatography coupled to MS/MS analysis, using a Xevo G2- XS QTof system (Waters
504 Corporation, USA). The separation method used is identical to the one used for muropeptide
505 separation explained below. A library of compounds was used to target the identification of
506 peptidoglycan precursors and possible intermediates, although only lipid II (lipid II-penta) was
507 detected in these samples. Lipid II amounts were calculated based on the integration of the peaks
508 (total area), normalized to the culture OD.

509 **Peptidoglycan (PG) purification and analysis**

510 PG samples were analyzed as described previously[54,55]. Briefly, 50 mL of WT and Δ*cdnL* cells
511 were grown to an OD_{600} of 0.5 in PYE, harvested, and boiled in 5% SDS for 2 h. Sacculi were
512 repeatedly washed with MilliQ water by ultracentrifugation (110,000 rpm, 10 min, 20 ºC) until
513 total removal of the detergent and finally treated with muramidase (100 µg/mL) for 16 hours at
514 37 ºC. Muramidase digestion was stopped by boiling and coagulated proteins were removed by
515 centrifugation (10 min, 14,000 rpm). For sample reduction, the pH of the supernatants was
516 adjusted to pH 8.5-9.0 with sodium borate buffer and sodium borohydride was added to a final
517 concentration of 10 mg/mL. After incubating for 30 min at room temperature, pH was adjusted
518 to 3.5 with orthophosphoric acid.

519 UPLC analyses of muropeptides were performed on a Waters UPLC system (Waters
520 Corporation, USA) equipped with an ACQUITY UPLC BEH C18 Column, 130Å, 1.7 µm, 2.1
521 mm X 150 mm (Waters, USA) and a dual wavelength absorbance detector. Elution of
522 muropeptides was detected at 204 nm. Muropeptides were separated at 45 °C using a linear
523 gradient from buffer A (formic acid 0.1% in water) to buffer B (formic acid 0.1% in acetonitrile)
524 in an 18-minute run, with a 0.25 mL/min flow. Relative total PG amounts were calculated by
525 comparison of the total intensities of the chromatograms (total area) from three biological
526 replicates normalized to the same OD_{600} and extracted with the same volumes. Muropeptide
527 identity was confirmed by MS/MS analysis, using a Xevo G2-XS QTof system (Waters
528 Corporation, USA). Quantification of muropeptides was based on their relative abundances
529 (relative area of the corresponding peak) normalized to their molar ratio.

530 **Metabolomics sample preparation and analysis**

531 4 mL of each strain was grown to an OD_{600} of 0.3 and filtered through 0.22 µm nylon filters
532 (Millipore GNWP04700). The filter was placed upside down in a 60 mm dish containing 1.2 mL
533 pre-chilled quenching solution (40:40:20 Acetonitrile:methanol:H_2O + 0.5% formic acid) and
534 incubated at -20 ºC for 15 minutes. Cells were washed off the filter by pipetting the quenching
535 solution over the filter, transferred to chilled bead beating tubes containing 50 mg of 0.1 mm
536 glass beads and neutralized with 100 µL 1.9M NH_4HCO. Cells were lysed on a beat beater using
537 a Qiagen Tissulyzer at 30Hz for 5 minutes. Samples were spun at 4 ºC for 5 min at max speed
538 and transferred to pre-chilled tubes to remove debris.

539 LC-MS analysis of cellular extract was conducted on Q Exactive PLUS Hybrid Quadrupole-
540 Orbitrap mass spectrometer (Thermo Fisher Scientific) using hydrophilic interaction
541 chromatography. The Dionex UltiMate 3000 UHPLC system (Thermo Fisher Scientific) with

542 XBridge BEH amide column (Waters, Milford, MA) and XP VanGuard Cartridge (Waters,
543 Milford, MA) were used for LC separation. The LC gradient, comprising solvent A (95%:5%
544 H2O:acetonitrile with 20 mM ammonium acetate, 20 mM ammonium hydroxide, pH 9.4) and
545 solvent B (20%:80% H2O:acetonitrile with 20 mM ammonium acetate, 20 mM ammonium
546 hydroxide, pH 9.4), corresponded with the following solvent B percentages over time: 0 min,
547 100%: 3 min, 100%; 3.2 min, 90%; 6.2 min, 90%; 6.5 min, 80%; 10.5 min, 80%; 10.7 min, 70%;
548 13.5 min, 70%; 13.7 min, 45%; 16 min, 45%; 16.5 min, 100%. Chromatography flow rate was at
549 300 µL/min and injection volume 5 µL. Column temperature was maintained at 25 °C. MS scans
550 were set to negative ion mode with a resolution of 70,000 at m/z 200, in addition to an automatic
551 gain control target of 3 x 10^6 and scan range of 72 to 1000. Metabolite data was obtained using
552 the MAVEN software package[56].
553

554 **References**

555 1. Österberg, S., Peso-Santos, T. del & Shingler, V. Regulation of Alternative Sigma Factor
556 Use. *Annu. Rev. Microbiol.* **65**, 37–55 (2011).
557 2. Stallings, C. L. *et al.* CarD Is an Essential Regulator of rRNA Transcription Required for
558 Mycobacterium tuberculosis Persistence. *Cell* **138**, 146–159 (2009).
559 3. Srivastava, D. B. *et al.* Structure and function of CarD, an essential mycobacterial
560 transcription factor. *Proc. Natl. Acad. Sci.* **110**, 12619–12624 (2013).
561 4. Weiss, L. A. *et al.* Interaction of CarD with RNA Polymerase Mediates Mycobacterium
562 tuberculosis Viability, Rifampin Resistance, and Pathogenesis. *J. Bacteriol.* **194**, 5621–
563 5631 (2012).
564 5. Gallego-García, A. *et al.* Structural Insights into RNA Polymerase Recognition and
565 Essential Function of Myxococcus xanthus CdnL. *PLOS ONE* **9**, e108946 (2014).
566 6. García-Moreno, D. *et al.* CdnL, a member of the large CarD-like family of bacterial
567 proteins, is vital for Myxococcus xanthus and differs functionally from the global
568 transcriptional regulator CarD. *Nucleic Acids Res.* **38**, 4586–4598 (2010).
569 7. Bae, B. *et al.* CarD uses a minor groove wedge mechanism to stabilize the RNA
570 polymerase open promoter complex. *eLife* **4**, e08505 (2015).
571 8. Typas, A., Banzhaf, M., Gross, C. A. & Vollmer, W. From the regulation of peptidoglycan
572 synthesis to bacterial growth and morphology. *Nat. Rev. Microbiol.* **10**, 123–136 (2012).
573 9. Cabeen, M. T. *et al.* Bacterial cell curvature through mechanical control of cell growth.
574 *EMBO J.* **28**, 1208–1219 (2009).
575 10. Woldemeskel, S. A. & Goley, E. D. Shapeshifting to Survive: Shape Determination and
576 Regulation in Caulobacter crescentus. *Trends Microbiol.* **25**, 673–687 (2017).

577 11. Gallego-García, A. *et al. Caulobacter crescentus* CdnL is a non-essential RNA polymerase-
578 binding protein whose depletion impairs normal growth and rRNA transcription. *Sci.*
579 *Rep.* **7**, 43240 (2017).
580 12. Sundararajan, K. *et al.* The bacterial tubulin FtsZ requires its intrinsically disordered
581 linker to direct robust cell wall construction. *Nat. Commun.* **6**, 7281 (2015).
582 13. Pincus, Z. & Theriot, J. A. Comparison of quantitative methods for cell-shape analysis. *J.*
583 *Microsc.* **227**, 140–156 (2007).
584 14. Seitz, L. C. & Brun, Y. V. Genetic Analysis of Mecillinam-Resistant Mutants ofCaulobacter
585 crescentus Deficient in Stalk Biosynthesis. *J. Bacteriol.* **180**, 5235–5239 (1998).
586 15. Figge, R. M., Divakaruni, A. V. & Gober, J. W. MreB, the cell shape-determining bacterial
587 actin homologue, co-ordinates cell wall morphogenesis in Caulobacter crescentus. *Mol.*
588 *Microbiol.* **51**, 1321–1332 (2004).
589 16. Takacs, C. N. *et al.* MreB Drives De Novo Rod Morphogenesis in Caulobacter crescentus
590 via Remodeling of the Cell Wall. *J. Bacteriol.* **192**, 1671–1684 (2010).
591 17. Dye, N. A., Pincus, Z., Fisher, I. C., Shapiro, L. & Theriot, J. A. Mutations in the nucleotide
592 binding pocket of MreB can alter cell curvature and polar morphology in Caulobacter.
593 *Mol. Microbiol.* **81**, 368–394 (2011).
594 18. Ausmees, N., Kuhn, J. R. & Jacobs-Wagner, C. The Bacterial Cytoskeleton: An
595 Intermediate Filament-Like Function in Cell Shape. *Cell* **115**, 705–713 (2003).
596 19. Barry, R. M. *et al.* Large-scale filament formation inhibits the activity of CTP synthetase.
597 *eLife* **3**, (2014).
598 20. Ingerson-Mahar, M., Briegel, A., Werner, J. N., Jensen, G. J. & Gitai, Z. The metabolic
599 enzyme CTP synthase forms cytoskeletal filaments. *Nat. Cell Biol.* **12**, 739–746 (2010).

600 21. Gonzalez, D. & Collier, J. Genomic Adaptations to the Loss of a Conserved Bacterial DNA
601 Methyltransferase. *mBio* **6**, e00952-15 (2015).
602 22. Dennis, G. *et al.* DAVID: Database for Annotation, Visualization, and Integrated
603 Discovery. *Genome Biol.* **4**, P3 (2003).
604 23. Hottes, A. K. *et al.* Transcriptional Profiling of Caulobacter crescentus during Growth on
605 Complex and Minimal Media. *J. Bacteriol.* **186**, 1448–1461 (2004).
606 24. Riley, R. G. & Kolodziej, B. J. Pathway of glucose catabolism in Caulobacter crescentus.
607 *Microbios* **16**, 219–226 (1976).
608 25. Stephens, C. *et al.* Genetic Analysis of a Novel Pathway for D-Xylose Metabolism in
609 Caulobacter crescentus. *J. Bacteriol.* **189**, 2181–2185 (2007).
610 26. Beaufay, F. *et al.* A NAD-dependent glutamate dehydrogenase coordinates metabolism
611 with cell division in Caulobacter crescentus. *EMBO J.* **34**, 1786–1800 (2015).
612 27. Doublet, P., Heijenoort, J. van, Bohin, J. P. & Mengin-Lecreulx, D. The murI gene of
613 Escherichia coli is an essential gene that encodes a glutamate racemase activity. *J.*
614 *Bacteriol.* **175**, 2970–2979 (1993).
615 28. Park, J. T. Why does Escherichia coli recycle its cell wall peptides? *Mol. Microbiol.* **17**,
616 421–426 (1995).
617 29. Ardissone, S. *et al.* Cell cycle constraints on capsulation and bacteriophage
618 susceptibility. *eLife* **3**, (2014).
619 30. Jorgenson, M. A., Kannan, S., Laubacher, M. E. & Young, K. D. Dead-end intermediates in
620 the enterobacterial common antigen pathway induce morphological defects in
621 Escherichia coli by competing for undecaprenyl phosphate. *Mol. Microbiol.* **100**, 1–14
622 (2016).

623 31. Jorgenson, M. A. & Young, K. D. Interrupting Biosynthesis of O Antigen or the
624 Lipopolysaccharide Core Produces Morphological Defects in Escherichia coli by
625 Sequestering Undecaprenyl Phosphate. *J. Bacteriol.* **198**, 3070–3079 (2016).
626 32. D'Elia, M. A. *et al.* Probing Teichoic Acid Genetics with Bioactive Molecules Reveals New
627 Interactions among Diverse Processes in Bacterial Cell Wall Biogenesis. *Chem. Biol.* **16**,
628 548–556 (2009).
629 33. Commichau, F. M., Forchhammer, K. & Stülke, J. Regulatory links between carbon and
630 nitrogen metabolism. *Curr. Opin. Microbiol.* **9**, 167–172 (2006).
631 34. Sperber, A. M. & Herman, J. K. Metabolism Shapes the Cell. *J. Bacteriol.* **199**, e00039-17
632 (2017).
633 35. Irnov, I. *et al.* Crosstalk between the tricarboxylic acid cycle and peptidoglycan
634 synthesis in Caulobacter crescentus through the homeostatic control of α-ketoglutarate.
635 *PLOS Genet.* **13**, e1006978 (2017).
636 36. Cabeen, M. T. & Jacobs-Wagner, C. Bacterial cell shape. *Nat. Rev. Microbiol.* **3**, 601–610
637 (2005).
638 37. Hill, N. S., Buske, P. J., Shi, Y. & Levin, P. A. A Moonlighting Enzyme Links Escherichia coli
639 Cell Size with Central Metabolism. *PLOS Genet.* **9**, e1003663 (2013).
640 38. Weart, R. B. *et al.* A metabolic sensor governing cell size in bacteria. *Cell* **130**, 335–347
641 (2007).
642 39. Radhakrishnan, S. K., Pritchard, S. & Viollier, P. H. Coupling Prokaryotic Cell Fate and
643 Division Control with a Bifunctional and Oscillating Oxidoreductase Homolog. *Dev. Cell*
644 **18**, 90–101 (2010).

645 40. Marks, M. E. *et al.* The Genetic Basis of Laboratory Adaptation in Caulobacter
646 crescentus. *J. Bacteriol.* **192**, 3678–3688 (2010).
647 41. Poindexter, J. S. Selection for Nonbuoyant Morphological Mutants of Caulobacter
648 crescentus. **135**, 5 (1978).
649 42. Woldemeskel, S. A., McQuillen, R., Hessel, A. M., Xiao, J. & Goley, E. D. A conserved coiled-
650 coil protein pair focuses the cytokinetic Z-ring in Caulobacter crescentus. *Mol.*
651 *Microbiol.* **105**, 721–740 (2017).
652 43. Paintdakhi, A. *et al.* Oufti: An integrated software package for high-accuracy, high-
653 throughput quantitative microscopy analysis. *Mol. Microbiol.* **99**, 767–777 (2016).
654 44. Schneider, C. A., Rasband, W. S. & Eliceiri, K. W. NIH Image to ImageJ: 25 years of image
655 analysis. *Nat. Methods* **9**, 671–675 (2012).
656 45. Schwender, H., Krause, A. & Ickstadt, K. Comparison of the Empirical Bayes and the
657 Significance Analysis of Microarrays. 26
658 46. Girardot, C., Scholtalbers, J., Sauer, S., Su, S.-Y. & Furlong, E. E. M. Je, a versatile suite to
659 handle multiplexed NGS libraries with unique molecular identifiers. *BMC Bioinformatics*
660 **17**, 419 (2016).
661 47. Li, H. & Durbin, R. Fast and accurate long-read alignment with Burrows–Wheeler
662 transform. *Bioinformatics* **26**, 589–595 (2010).
663 48. Li, H. *et al.* The Sequence Alignment/Map format and SAMtools. *Bioinformatics* **25**,
664 2078–2079 (2009).
665 49. Robinson, J. T. *et al.* Integrative Genomics Viewer. *Nat. Biotechnol.* **29**, 24–26 (2011).

666 50. Thorvaldsdóttir, H., Robinson, J. T. & Mesirov, J. P. Integrative Genomics Viewer (IGV):
667 high-performance genomics data visualization and exploration. *Brief. Bioinform.* **14**,
668 178–192 (2013).
669 51. McCarthy, D. J., Chen, Y. & Smyth, G. K. Differential expression analysis of multifactor
670 RNA-Seq experiments with respect to biological variation. *Nucleic Acids Res.* **40**, 4288–
671 4297 (2012).
672 52. Robinson, M. D., McCarthy, D. J. & Smyth, G. K. edgeR: a Bioconductor package for
673 differential expression analysis of digital gene expression data. *Bioinformatics* **26**, 139–
674 140 (2010).
675 53. Qiao, Y. *et al.* Lipid II overproduction allows direct assay of transpeptidase inhibition by
676 β-lactams. *Nat. Chem. Biol.* **13**, 793–798 (2017).
677 54. Alvarez, L., Hernandez, S. B., de Pedro, M. A. & Cava, F. Ultra-Sensitive, High-Resolution
678 Liquid Chromatography Methods for the High-Throughput Quantitative Analysis of
679 Bacterial Cell Wall Chemistry and Structure. in *Bacterial Cell Wall Homeostasis: Methods*
680 *and Protocols* (ed. Hong, H.-J.) 11–27 (Springer New York, 2016). doi:10.1007/978-1-
681 4939-3676-2_2
682 55. Desmarais, S. M., Pedro, M. A. D., Cava, F. & Huang, K. C. Peptidoglycan at its peaks: how
683 chromatographic analyses can reveal bacterial cell wall structure and assembly. *Mol.*
684 *Microbiol.* **89**, 1–13 (2013).
685 56. Melamud, E., Vastag, L. & Rabinowitz, J. D. Metabolomic analysis and visualization
686 engine for LC-MS data. *Anal. Chem.* **82**, 9818–9826 (2010).
687

688 **Acknowledgements**

689 We thank members of the Goley lab for helpful discussions and input. We thank Kousik
690 Sundararajan for identifying the initial mutant of CdnL that suppresses the FtsZΔCTL
691 phenotype. We would like to thank Julie Theriot, Lucy Shapiro, Christine Jacobs-Wagner, Regis
692 Hallez, and Zemer Gitai for providing materials and strains used in this project. We thank the
693 Johns Hopkins Genetic Resources Core Facility for RNA-Seq services and analysis, Zach Pincus
694 for guidance in using CellTool and the Metabolomics core at the Rutgers Cancer Institute of
695 New Jersey for metabolomics analysis. This work was funded by the NIH through
696 R01GM108640 (to EDG), R01GM111706 (to PC), T32GM08515 (training grant support of RZ),
697 and T32GM007445 (training grant support of AKD) and Johns Hopkins Discovery Fund grant to
698 EDG. JC is funded by Swiss National Science Foundation (SNSF) grants 31003A_140758 and
699 31003A_173075. Research in the Cava lab is supported by MIMS, the Knut and Alice
700 Wallenberg Foundation (KAW), the Swedish Research Council, and the Kempe Foundation.

701

702

703 **Author contributions**

704 SAW and EDG conceived the study. SAW, LA, RZ, DG, JC, PC, FC, and EDG designed the
705 experiments. SAW performed the majority of experiments and analysis, except as noted. LA
706 performed muropeptide analysis and lipid II quantification. SAW, AKD, RZ, and PC performed
707 and/or analyzed Tn-Seq experiments. AB wrote custom software to analyze MreB distribution.
708 DG performed and analyzed microarray experiments. EDG purified CdnL, generated strains, and
709 performed CellTool analysis of shape. JC, PC, FC, and EDG supervised the research. SAW and
710 EDG wrote the manuscript with support and editing from all authors.

711 **Figure and Legends**

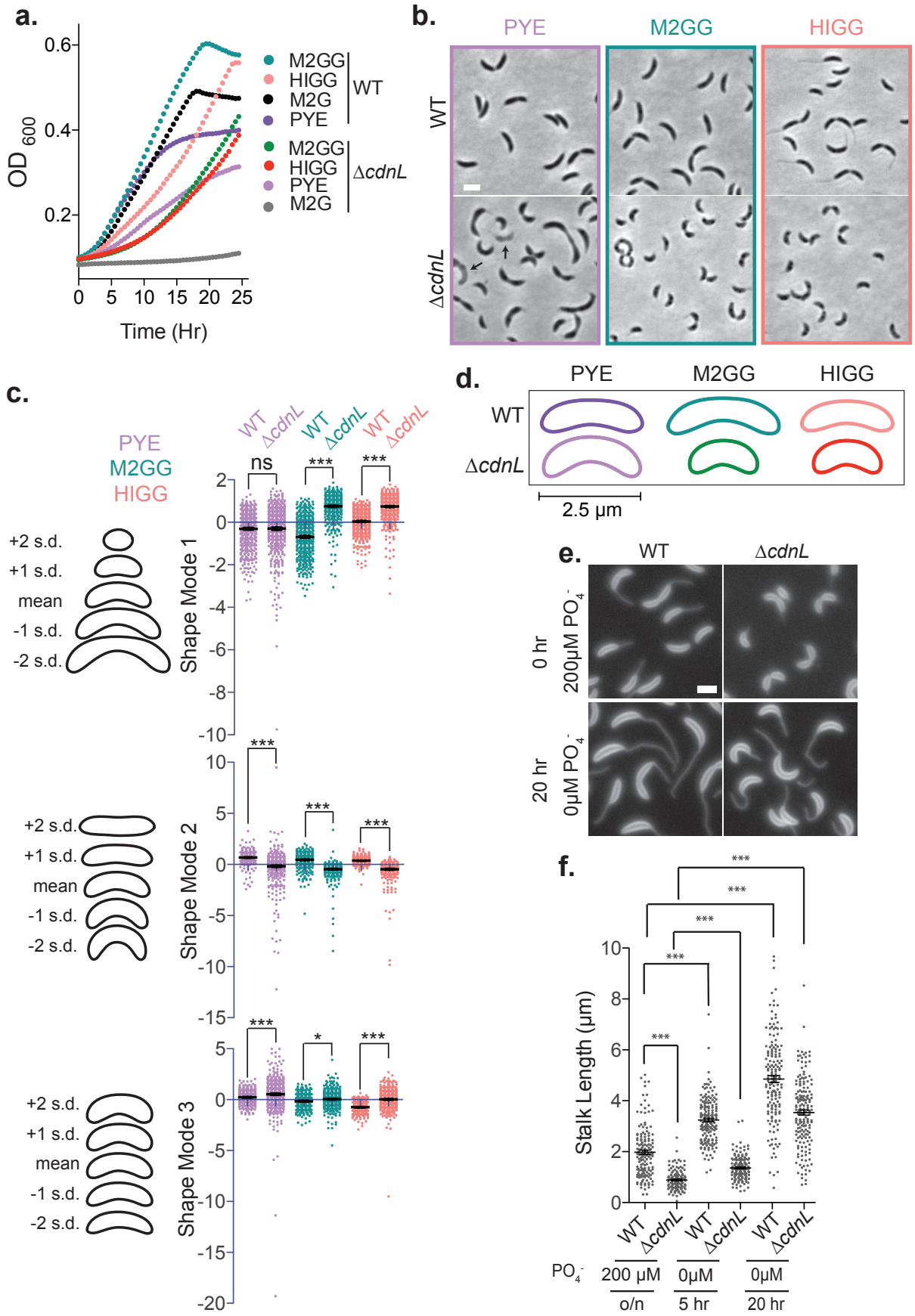
a.
OD 600
Time (Hr)
M2GG
HIGG
M2G
PYE
WT
M2GG
HIGG
PYE
M2G
ΔcdnL
b.
PYE
M2GG
HIGG
WT
ΔcdnL
c.
PYE
M2GG
HIGG
WT
ΔcdnL
ns
***
+2 s.d.
+1 s.d.
mean
-1 s.d.
-2 s.d.
Shape Mode 1
Shape Mode 2
Shape Mode 3
*
d.
PYE
M2GG
HIGG
WT
ΔcdnL
2.5 µm
e.
WT
ΔcdnL
0 hr
200µM PO4-
20 hr
0µM PO4-
f.
Stalk Length (µm)
WT
ΔcdnL
PO4-
200 µM
0µM
0µM
o/n
5 hr
20 hr

713 **Figure 1: Cells lacking CdnL have pleiotropic morphological and growth defects. a**. Growth
714 of WT (EG865) and Δ*cdnL* (EG1447) cells in the indicated media. **b.** Phase contrast images of
715 WT and Δ*cdnL* cells grown in the indicated media. Arrows indicate ghost cells. Bar = 2 µm. **c.**
716 PCA of cell shape for WT and Δ*cdnL* shown in **b.** Scatter plots of shape modes 1, 2 and 3
717 approximately correspond to length, curvature and width. Contours on the left of scatter plots
718 indicate mean cell shape and standard deviations (s.d) from the mean. **d.** Mean shapes of WT and
719 Δ*cdnL* cells grown in the indicated media. **e.** Membrane staining of WT (EG865) and Δ*cdnL*
720 (EG1447) cells with FM4-64 after growth in HIGG media with and without phosphate. **f.** Stalk
721 lengths measured using ImageJ's[44] line tool. Mean and SEM included for plots in **c.** and **f.**
722 Statistical analysis in **c.** and **f.** performed using one-way ANOVA with Bonferroni's Multiple
723 Comparison Test, n = 500 for each in **c.** n = 150, 127, 168, 155, 162, 172 from left to right in **e.**
724 *** = $p < 0.001$, * = $p < 0.05$, ns = not significant.
725

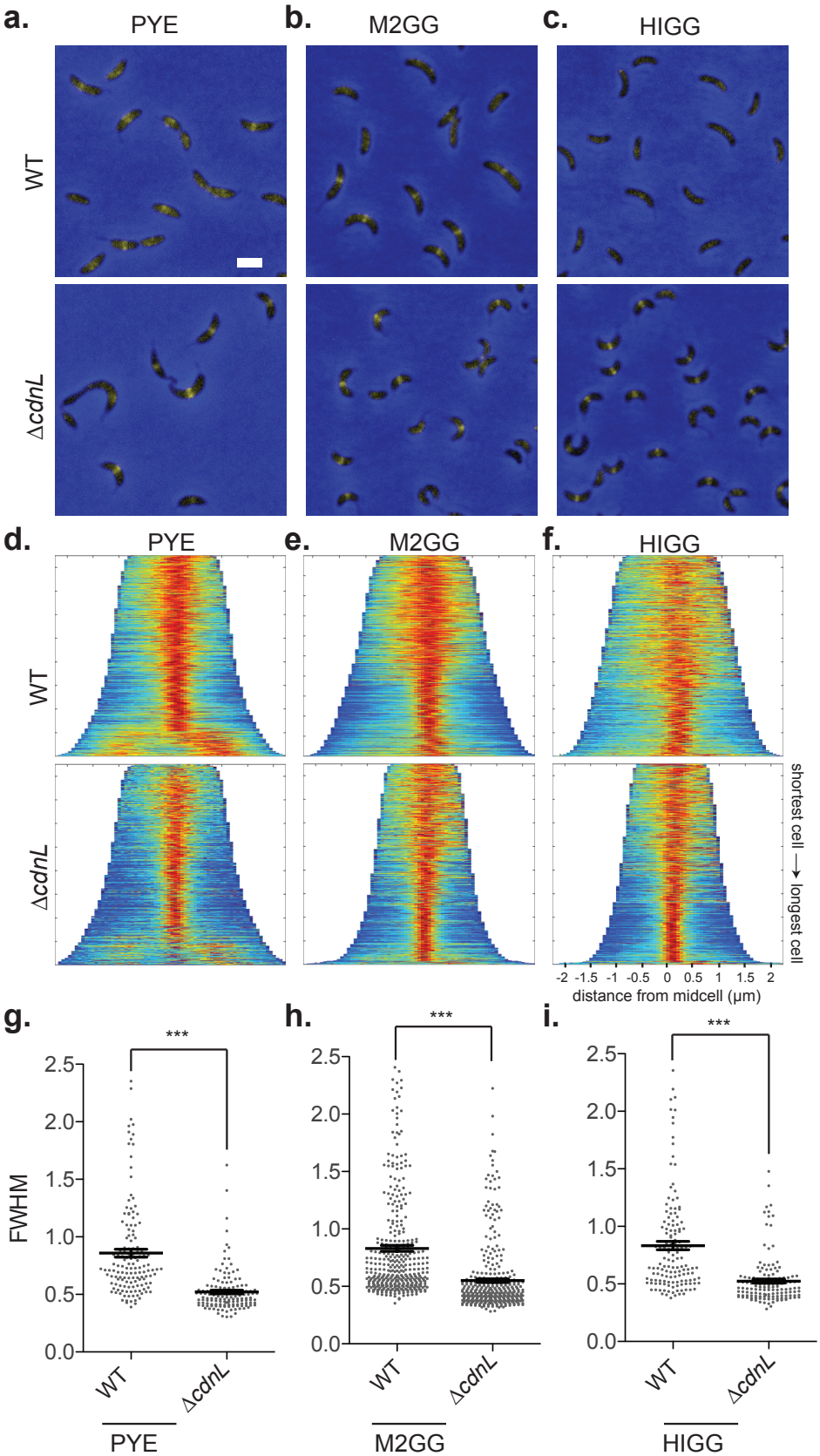
a.
PYE
b.
M2GG
c.
HIGG
WT
ΔcdnL
d.
PYE
e.
M2GG
f.
HIGG
WT
ΔcdnL
shortest cell → longest cell
-2 -1.5 -1 -0.5 0 0.5 1 1.5 2
distance from midcell (μm)
g.
h.
i.
FWHM
2.5
2.0
1.5
1.0
0.5
0.0
***
WT
ΔcdnL
PYE
M2GG
HIGG

727 **Figure 2: MreB localization is aberrant in Δ*cdnL* cells. a, b & c.** Merged phase contrast (blue)
728 and fluorescence (yellow) images of WT (EG1795) and Δ*cdnL* cells (EG2465) expressing *venus-*
729 *mreB* for 2 hrs from the *xylX* promoter in the indicated media. Bar = 2 µm. **d, e & f.** Demographs
730 of images shown in **a, b &c.** n = 850 cells for each. **g, h & i.** Scatter plots of full width at half
731 maximum (FWHM) values of midcell-localized MreB. Cell length range used for FWHM
732 calculation of midcell-localized MreB was determined from demographs shown in **d-f**. For PYE,
733 WT and Δ*cdnL*, cells 2 – 3 µm long have MreB localized at midcell and were selected for
734 FWHM calculations. For M2GG, WT and Δ*cdnL* cells between lengths of 3 – 3.75 µm and 2 – 3
735 µm, respectively, were selected for FWHM calculations. For HIGG, WT and Δ*cdnL* cells
736 between lengths of 3 – 3.5 µm and 2 – 3 µm, respectively, were selected for FWHM
737 calculations. Statistical analysis performed using unpaired t test. *** = $p < 0.001$. n = 140 each
738 for PYE and HIGG and n = 383 each for M2GG.
739

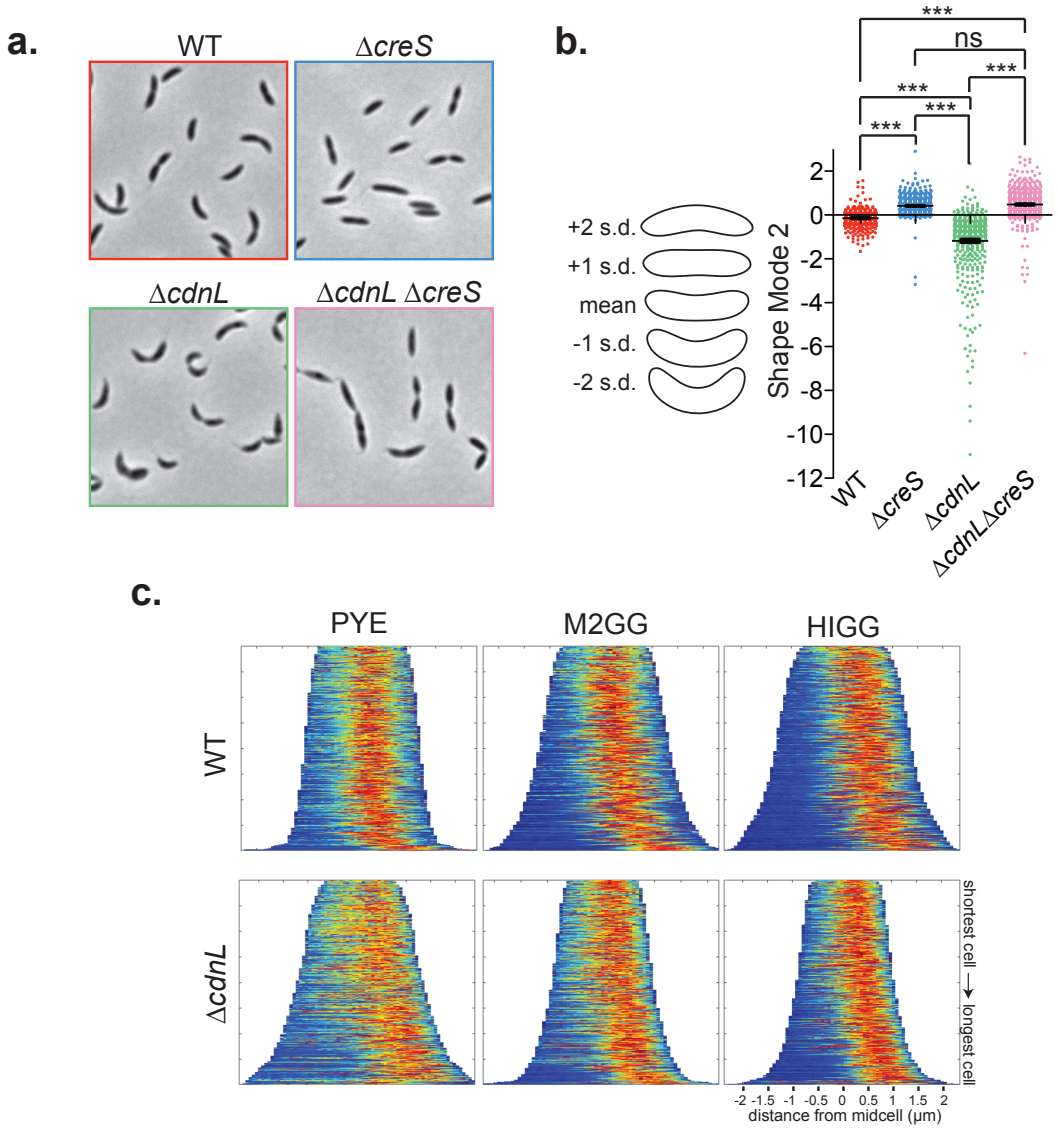

740

741 **Figure 3: Hypercurvature of Δ*cdnL* cells is dependent on crescentin and may involve CTP**

742 **synthase. a.** Phase contrast images of WT (EG865), Δ*creS* (EG1903), Δ*cdnL::gentR* (EG1898)

743 and Δ*creS* Δ*cdnL::gentR* (EG1912). **b.** Scatter plot depicting shape mode 2 (~curvature) from

744 PCA of cell shape for cells shown in **a**. Mean and SEM values are indicated. n = 447, 615, 734,

745 574 from left to right. Contours on the left of scatter plots indicate mean cell shape and standard

746 deviations (s.d) from the mean. Statistical analysis performed using one-way ANOVA with

747 Bonferroni's Multiple Comparison Test. *** = $p < 0.001$, ns = not significant. **c.** Demographs of

748 images from Supplementary Figure 3 of WT (EG1902) and Δ*cdnL* (EG1958) cells expressing

749 *mCherry – ctpS* from the *xylX* locus grown in indicated media. n = 400 cells for each.

750

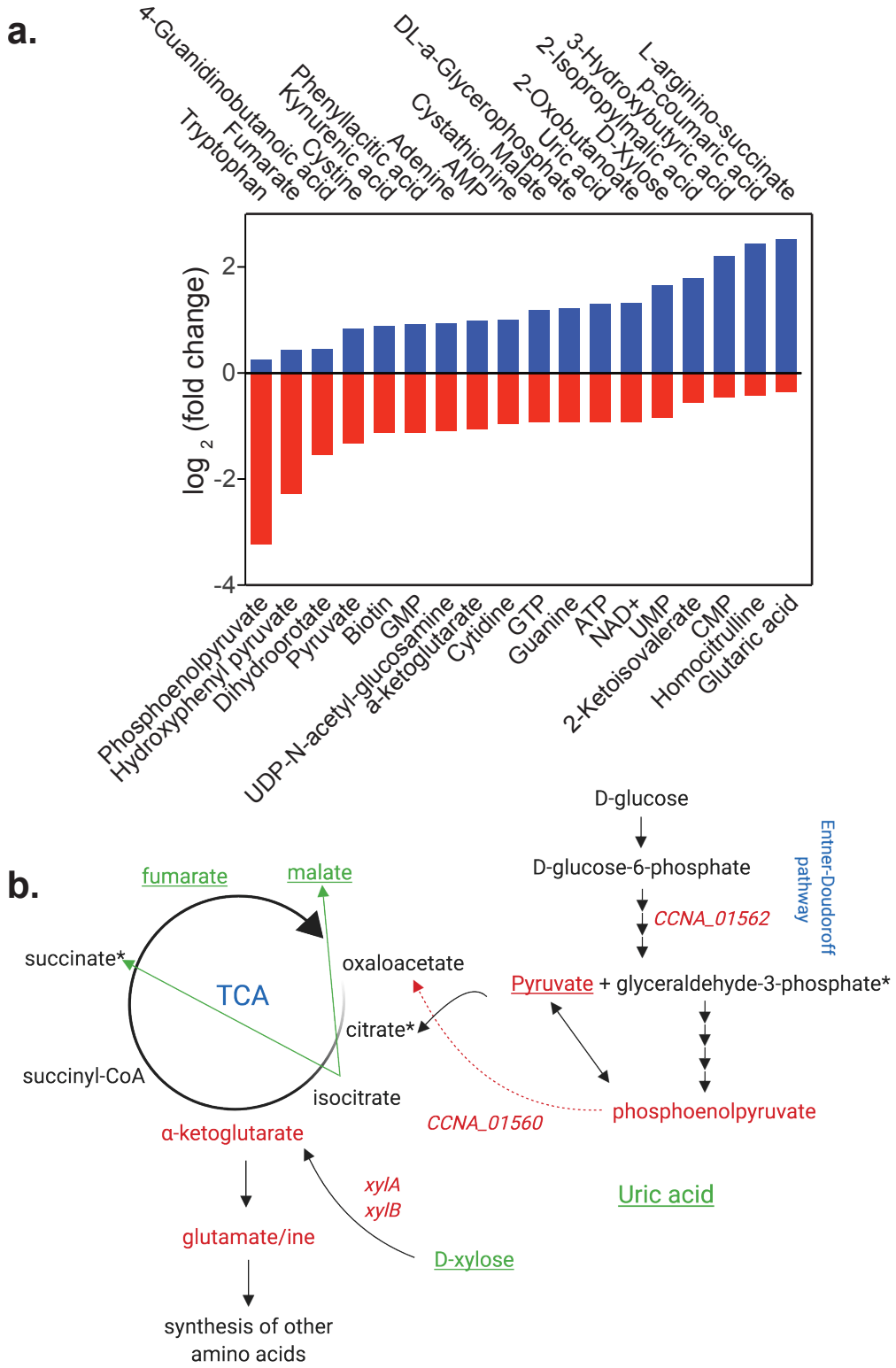

751

752 **Figure 4: CdnL is required for metabolic homeostasis in *Caulobacter***

753 **a.** Graph showing significantly altered metabolites ($p < 0.05$) in Δ*cdnL* compared to WT grown
754 in PYE from Supplementary table 3. **b.** Summary figure depicting changes in glucose
755 metabolism and TCA cycle in Δ*cdnL* cells as compared to WT. Genes and metabolites shown in
756 red are downregulated and in green are upregulated. Underlined metabolites are changed across
757 all media types, whereas those in black are unchanged. * indicates metabolites not detected. n =
758 3 for each strain in each condition.
759

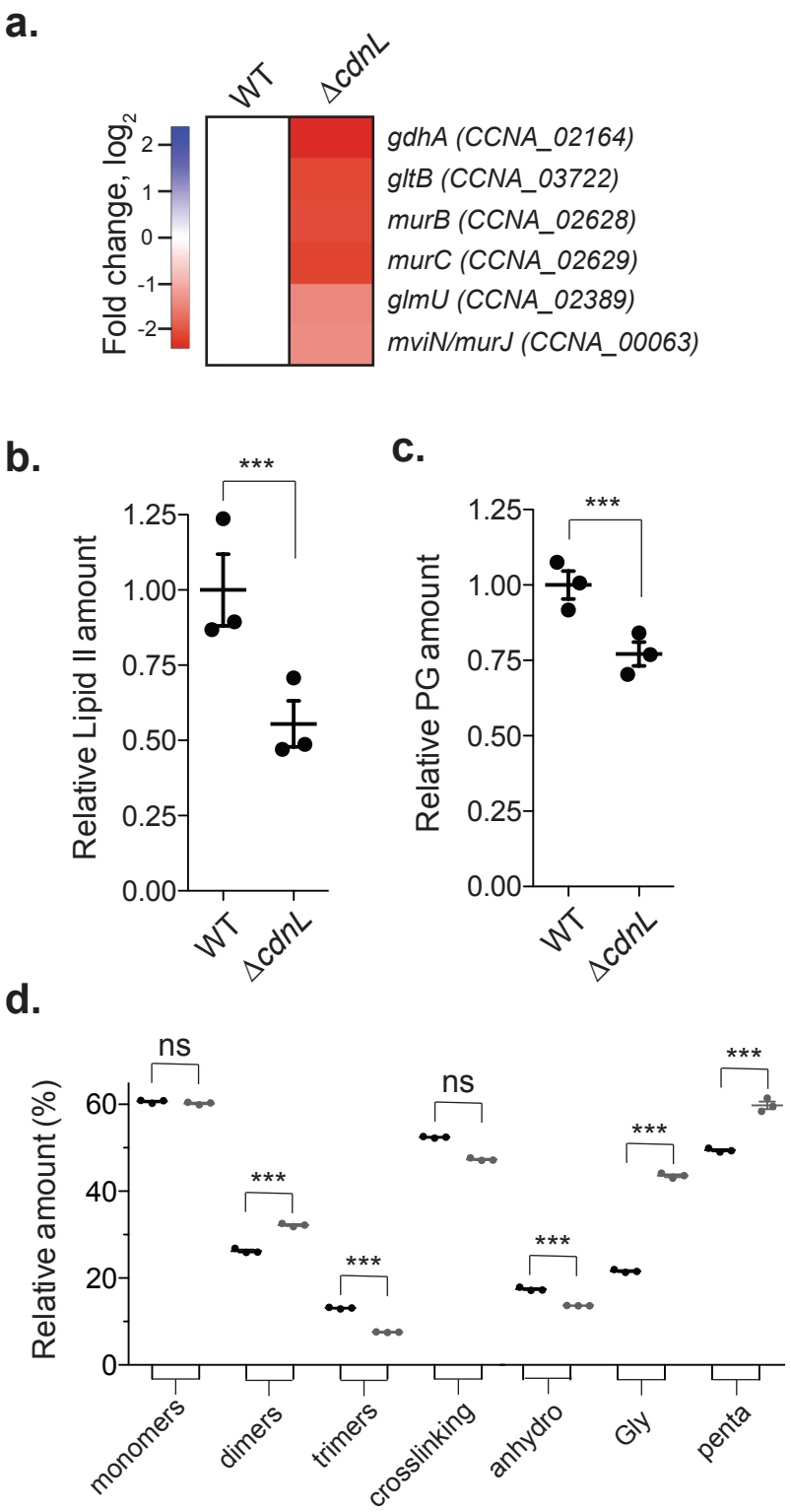
a.
WT
ΔcdnL
Fold change, log2
2
1
0
-1
-2
gdhA (CCNA_02164)
gltB (CCNA_03722)
murB (CCNA_02628)
murC (CCNA_02629)
glmU (CCNA_02389)
mviN/murJ (CCNA_00063)
b.
***
Relative Lipid II amount
1.25
1.00
0.75
0.50
0.25
0.00
WT
ΔcdnL
c.
***
Relative PG amount
1.25
1.00
0.75
0.50
0.25
0.00
WT
ΔcdnL
d.
ns
***
ns
***
***
***
***
Relative amount (%)
60
40
20
0
monomers
dimers
trimers
crosslinking
anhydro
Gly
penta

760

761 **Figure 5: CdnL impacts cell wall precursor synthesis and cell wall metabolism. a.** Heatmap
762 showing changes of the indicated transcripts involved in lipid II synthesis and cell wall
763 remodeling in WT (EG865) and Δ*cdnL* (EG1415) using RNA-Seq. **b. & c.** Relative amount of
764 lipid II and peptidoglycan in WT (EG865) and Δ*cdnL* (EG1447) cells. **d.** Indicated muropeptide
765 species from WT (EG865) and Δ*cdnL* (EG1447). X-axis shown in **d** are (1-6 anhydro) N-acetyl
766 muramic acid (anhydro), Gly containing muropeptides (Gly), and pentapeptides (penta). Values
767 in **b, c, & d** are from three independent cultures and mean and SEM are indicated. Statistical
768 analysis performed using unpaired t test. *** = $p < 0.001$, ** = $p < 0.01$, * = $p < 0.05$.
769

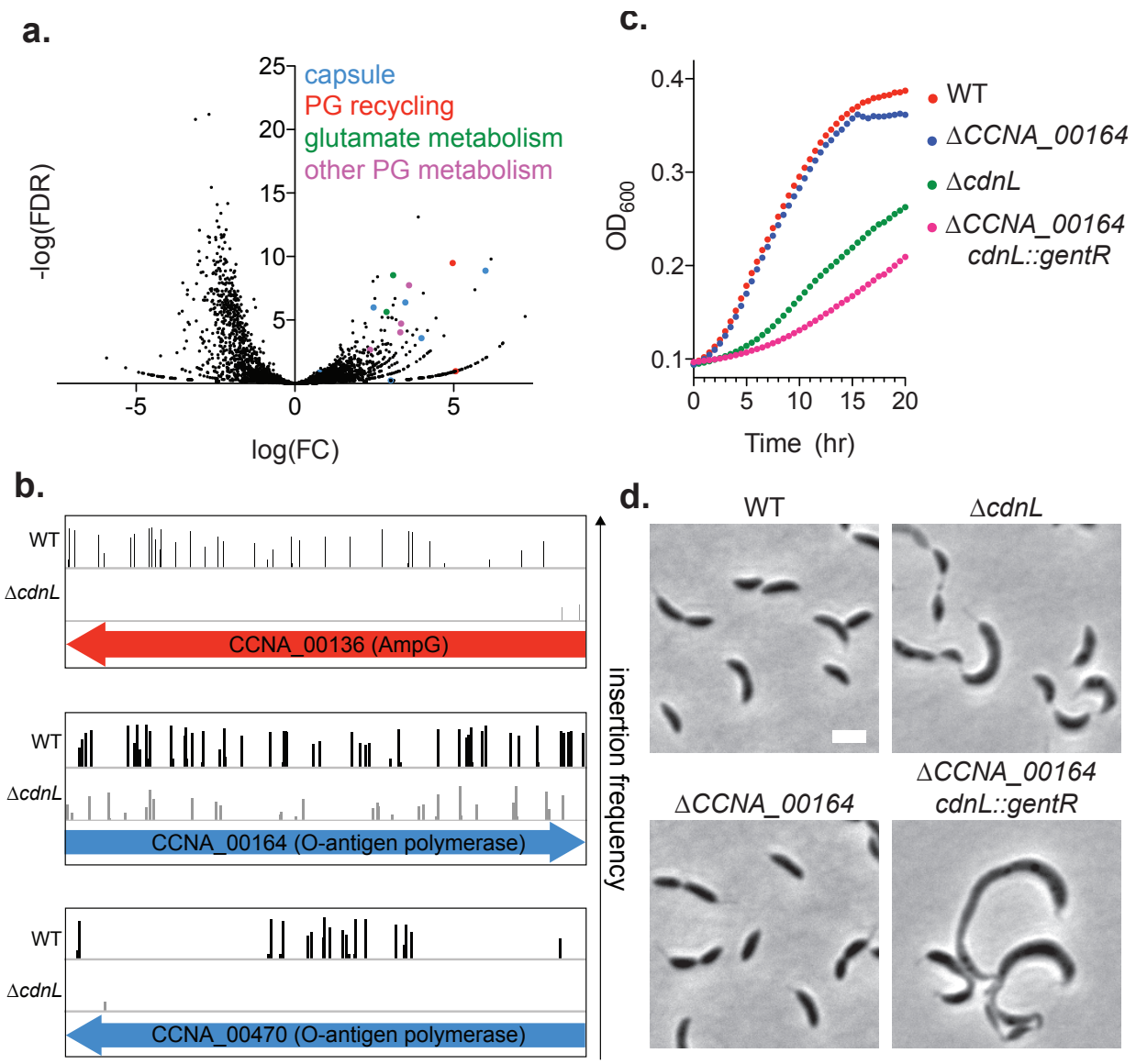

Figure 6: Mutations in cell wall recycling and capsule biosynthetic genes are synthetic lethal with Δ*cdnL*. a. Volcano plot representation of Tn-Seq analysis, WT/Δ*cdnL*. Negative $\log_{10}$ of the false discovery rate (-log(FDR)) is plotted against $\log_2$ of the fold change in number of unique transposon insertions in each gene in WT (EG865) vs Δ*cdnL* (EG1447). Genes that become essential in the Δ*cdnL* background and are discussed in this study are color-coded. **b.** Transposon insertion profile for selected genes from **a. c & d.** Growth curves and phase contrast

777 images for WT (EG865), Δ*cdnL* (EG1447), Δ*CCNA_00164* (EG2604) and *cdnL::gentR*

778 Δ*CCNA_00164* (EG2804). Bar = 2 μm.

779

780

781

782
783

784